Available online at www.sciencedirect.com
SCIENCE DIRECT®
Journal of Computational Physics 206 (2005) 453–462
JOURNAL OF COMPUTATIONAL PHYSICS
www.elsevier.com/locate/jcp

A multi-relaxation lattice kinetic method for passive scalar diffusion

Igor Rasin [a,*], Sauro Succi [b], Wolfram Miller [a]

[a] *Institute for Crystal Growth (IKZ), Max-Born-Str. 2, 12489 Berlin, Germany*
[b] *Istituto Applicazioni Calcolo CNR, 137 Viale Policlinico, 00144 Rome, Italy*

Received 21 July 2004; received in revised form 30 November 2004; accepted 20 December 2004
Available online 29 January 2005

Abstract

A kinetic Lattice-Boltzmann scheme for advection–diffusion is presented. The scheme is based on a matrix formulation of the lattice Boltzmann method which permits to handle *non-isotropic* diffusion–advection problems. In addition, by adjusting the kinetic eigenvectors defining the collision matrix to the local value of the flow velocity, the scheme is also shown to preserve isotropy under genuinely two-dimensional flow.

Keywords: Lattice Boltzmann method; Advection–diffusion equation; Modified Lax-Wendroff finite-difference scheme; Non-isotropic diffusion; Taylor–Aris dispersion

1. Introduction

In the recent years the lattice Boltzmann (LB) method has met with increasing interest as an alternative to the discretization of the Navier–Stokes equations for the numerical simulation of complex flows [1–5]. Many complex flow applications involve the dynamical evolution of chemical species which advect and diffuse without any appreciable effect on the dynamics of the fluid flow (passive scalars). Examples in point are the spreading of contaminants in groundwater, tracer dispersion in rough fractures, flows with phase transitions and many others. Many schemes are currently available to couple the dynamics of passive scalars to LB methods for fluid flows, ranging from recent variants of the finite-difference Lax-Wendroff schemes [6], to lattice kinetic schemes [7–10] and stochastic particle methods [11]. As a general rule, kinetic schemes are very

* Corresponding author.
E-mail address: rasin@ikz-berlin.de (I. Rasin).

0021-9991/$ - see front matter
doi:10.1016/j.jcp.2004.12.010

appealing because they move information along pre-defined, constant characteristics rather than along a space-time changing flow field. Furthermore, diffusion is not represented by second order spatial derivatives, but rather in the form of adiabatic relaxation to a local equilibrium. As a result, the time-step scales only linearly with mesh size, rather than quadratically. On the other hand, since the passive scalar is represented through a set of (at least) $2d$ populations in d dimensions, kinetic schemes imply a certain overhead in terms of memory occupation which must be weighed against the gains in timestep size.

In this note, we present a matrix extension of lattice kinetic schemes which can handle non isotropic problems as well as cure spurious directional effects in isotropic ones without introducing any further memory overhead.

2. Kinetic finite-difference method

We shall be concerned with the following advection–diffusion equation:

$$\partial_t \rho + \nabla \cdot (\rho \vec{u}) = \nabla \cdot D \nabla \rho, \tag{1}$$

where ρ is the concentration of the passive scalar, $\vec{u}$ is the flow velocity and D is the diffusion coefficient, generally a function of coordinates $D = D(\vec{r})$.

Explicit finite-difference schemes for the above equation are subject to conditional stability constraints connected with value of the dimensionless diffusion and advection coefficients $D^* = D\delta_t/\delta_x^2$ and $u^* = u\delta_t/\delta_x$ (also known as diffusive and convective Courant numbers), where δ_x and δ_t are the mesh spacing and lattice time-step, respectively. For instance, in the case of the two-dimensional modified Lax-Wendroff (MLW) scheme these constraints take the form [6,12]

$$D^* + \tfrac{1}{2}u^{*2} < \tfrac{1}{4}, \quad 2D^* > \max_{(x,y)}\{-u_x^{*2} + |u_x^*|, -u_y^{*2} + |u_y^*|\}.$$

The former refers to amplitude errors, and controls stability and numerical diffusion. The latter associates with phase errors and controls numerical dispersion.

Since D^* is scaled with δ_x^2/δ_t, it is clear that such stability conditions are very restrictive for the time step, as they scale with the square of the lattice spacing. It is therefore of interest to seek for alternative numerical schemes, free from such a restriction. Kinetic methods represent such an option. The main idea of kinetic methods is to replace the parabolic equation by a hyperbolic super-set of equations, so that diffusion results as an *emergent property* of relaxation to local equilibrium, and needs not be represented by any second order spatial derivative (the cause of the quadratic time-step scaling).

The governing kinetic Boltzmann equation for f_i takes the following relaxation form (in lattice units $\delta_t = \delta_x = 1$):

$$f_i(\vec{r} + \vec{c}_i, t+1) = f_i(\vec{r}, t) + \sum_j \Omega_{ij}(f_j^{\mathrm{eq}} - f_j), \tag{2}$$

where f_i represents the probability to find a particle with speed $\vec{c}_i$ at position $\vec{r}$ and time t.

The discrete speeds $\vec{c}_i$ describe the finite-difference template of the kinetic scheme. In the following, we shall deal with simple nearest-neighbor connections, that is:

$$\vec{c}_1 = (1,0), \quad \vec{c}_2 = (0,1), \quad \vec{c}_3 = (-1,0), \quad \vec{c}_4 = (0,-1),$$

in units of the lattice spacings, that is $\vec{c}_1\delta_x = (\delta_x, 0),\ \vec{c}_2\delta_y = (0, \delta_y)$.

The concentration ρ and flux $\mathbf{J}$ values are related to f_i in the following way:

$$\rho = \sum_i f_i, \quad \mathbf{J}_\alpha = \sum_i c_{i\alpha} f_i, \quad \alpha = 1,2 \text{ – spatial index.} \tag{3}$$

In Eq. (2) Ω is a relaxation matrix [13] which defines how quickly the local distribution function f_i relaxes towards the equilibrium value f_i^{eq}.

Taylor expansion of Eq. (2) yields the system of two hyperbolic equations for ρ and $\vec{\mathbf{J}}$:

$$\dot{\rho} + \nabla_\alpha \mathbf{J}_\alpha + \frac{1}{2}\ddot{\rho}_i + \nabla_\alpha \dot{\mathbf{J}}_\alpha + \frac{1}{2}\nabla_\alpha \nabla_\beta \mathbf{P}_{\alpha\beta} = \sum_{ij} \Omega_{ij}(f_j^{\mathrm{eq}} - f_j), \tag{4}$$

$$\dot{\mathbf{J}}_\alpha + \nabla_\beta \mathbf{P}_{\alpha\beta} + \frac{1}{2}\ddot{\mathbf{J}}_\alpha + \nabla_\beta \dot{\mathbf{P}}_{\alpha\beta} + \frac{1}{2}\nabla_\beta \nabla_\gamma \mathbf{M}_{\alpha\beta\gamma} = \sum_{ij} c_{i\alpha}\Omega_{ij}(f_j^{\mathrm{eq}} - f_j), \tag{5}$$

where $\mathbf{P}_{\alpha\beta} \equiv \sum_i c_{i\alpha}c_{i\beta}f_i$, $\mathbf{M}_{\alpha\beta\gamma} \equiv \sum_i c_{i\alpha}c_{i\beta}c_{i\gamma}f_i$ are higher order kinetic moments. In the above, dot stands for time-derivative and repeated indices are summed upon.

Furthermore, we posit that density is conserved and current density on a tensorial inverse time scale $\Lambda_{\alpha\beta}$. In other words, collisions realize the following relaxation dynamics $\delta\rho/\delta t = 0$ and $\delta J_\alpha/\delta t = -\Lambda_{\alpha\beta}(J_\beta - J_\beta^{\mathrm{eq}})$. This implies the following algebraic constraints:

$$\sum_i \Omega_{ij} = 0, \quad \sum_i c_{i\alpha}\Omega_{ij} = \sum_\beta \Lambda_{\alpha\beta}c_{j\beta},$$

where $\Lambda_{\alpha\beta}$ are free parameters to be fine-tuned to obtain the desired macroscopic equations.

Using these properties, we obtain:

$$\dot{\rho} + \nabla_\alpha \mathbf{J}_\alpha + \tfrac{1}{2}\ddot{\rho}_i + \nabla_\alpha \dot{\mathbf{J}}_\alpha + \tfrac{1}{2}\nabla_\alpha \nabla_\beta \mathbf{P}_{\alpha\beta} = 0, \tag{6}$$

$$\dot{\mathbf{J}}_\alpha + \nabla_\beta \mathbf{P}_{\alpha\beta} + \tfrac{1}{2}\ddot{\mathbf{J}}_\alpha + \nabla_\beta \dot{\mathbf{P}}_{\alpha\beta} + \tfrac{1}{2}\nabla_\beta \nabla_\gamma \mathbf{M}_{\alpha\beta\gamma} = \Lambda_{\alpha\beta}(\mathbf{J}_\beta^{\mathrm{eq}} - \mathbf{J}_\beta). \tag{7}$$

Since mass is conserved, and momentum is not, we make the following assumption:

$$\rho^{\mathrm{eq}} = \rho, \quad \mathbf{J}_\alpha \neq \mathbf{J}_\alpha^{\mathrm{eq}} = \rho u_\alpha.$$

This choice delivers the following expression for f_i^{eq}:

$$f_i^{\mathrm{eq}} = w_i \rho \left(1 + \frac{1}{c_s^2} u_\alpha^* c_{i\alpha}\right),$$

where $w_i = [1/4,\ 1/4,\ 1/4,\ 1/4]$ and $c_s^2 = \sum_i w_i c_{ix}^2 = \sum_i w_i c_{iy}^2 = 1/2$ is the lattice sound speed.

Next, we assume that $\mathbf{P}$ and $\mathbf{M}$ are near their equilibrium values:

$$\mathbf{P}_{\alpha\beta} \approx \mathbf{P}_{\alpha\beta}^{\mathrm{eq}} = \rho c_s^2 \delta_{\alpha\beta}, \quad \mathbf{M}_{\alpha\beta\gamma} \approx \mathbf{M}_{\alpha\beta\gamma}^{\mathrm{eq}} = \rho c_s^2 u_\delta^* \delta_{\alpha\beta\gamma\delta}.$$

Thus, in the continuum limit and within the near-equilibrium approximation, the discrete equation (2) goes towards the non-isotropic advection–diffusion equation in conservative form

$$\dot{\rho} + \nabla \cdot (\rho \vec{u}) = \nabla_\alpha (D_{\alpha\beta} \nabla_\beta \rho) \tag{8}$$

with the tensor diffusivity defined by the following expression:

$$D_{\alpha\beta}^* \equiv \left(\tfrac{1}{2}\delta_{\alpha\gamma} - u_\alpha^* u_\gamma^*\right)\left((\Lambda^{-1})_{\gamma\beta} - \tfrac{1}{2}\delta_{\gamma\beta}\right). \tag{9}$$

Note that, due to the conservative form of Eq. (8), this tensor diffusivity may exhibit an explicit spatial dependence. The relation (9) fixes the relaxation matrix $\Lambda_{\alpha\beta}$ in terms of the prescribed diffusion tensor $D_{\alpha\beta}$. It is important to remark that the flow-dependent correction $u_\alpha u_\gamma$ in the above equation stems from the *dia*batic term $\partial_{tt}\rho$ which is implicitly contained in Eq. (7). This flow-dependent (non-isotropic) effect can be reabsorbed into an isotropic diffusivity by appropriate tuning of the scattering matrix Λ. From Eq. (9) it is clear that, unless one moves to higher-order connectivity lattices (see Appendix A), such a

recovery can only be obtained within a matrix LB formulation. For the case of isotropic diffusion, $D_{\alpha\beta} = D\delta_{\alpha\beta}$, the matrix Λ reads as follows:

$$\Lambda = \frac{2}{(1+4D^*)\lambda}\begin{bmatrix} \lambda - 8D^*u_x^{*2} & -8D^*u_x^*u_y^* \\ -8D^*u_x^*u_y^* & \lambda - 8D^*u_y^{*2} \end{bmatrix}, \quad \lambda \equiv 1 + 4D^* - 2u^{*2}. \tag{10}$$

It is worth emphasizing that even for the case of isotropic diffusion, this matrix cannot be diagonal unless the flow is locally one-dimensional, that is $u_x u_y = 0$. The collision matrix can then be built according to a (generalized) spectral decomposition [8,14]

$$\Omega_{ij} = w_i \sum_{k=1}^{2} \frac{V_i^{(k)}}{N_k} \sum_{l=1}^{2} \Lambda_{kl} V_j^{(l)} + w_i \lambda_3 \frac{V_i^{(3)} V_j^{(3)}}{N_3},$$

where $V_i^{(1)} = c_{ix}$, $V_i^{(2)} = c_{iy}$, $V_i^{(3)} = c_{ix}^2 - c_{iy}^2$ are orthogonal eigenvectors and $N_k = \sum_i V_i^{(k)} w_i V_i^{(k)}$ are normalization factors. Note that the collision matrix projects zero on the first eigenvector $V_i^{(0)} = 1$ because of mass conservation.

The explicit form of the collision matrix is

$$\Omega = \frac{1}{2}\begin{bmatrix} \Lambda & -\Lambda \\ -\Lambda & \Lambda \end{bmatrix} + \frac{\lambda_3}{4}\begin{bmatrix} P_3 & P_3 \\ P_3 & P_3 \end{bmatrix}, \tag{11}$$

where Λ denotes the 2×2 block $\Lambda_{\alpha\beta}$ and $P_3 = \begin{bmatrix} 1 & -1 \\ -1 & 1 \end{bmatrix}$ is the projector associated with the third eigenvector.

The eigenvalues of the matrix Ω are:

$$\lambda_0 = 0, \quad \lambda_1 = \frac{2}{1+4D^*}, \quad \lambda_2 = \frac{2(1-2u^{*2})}{1+4D^*-2u^{*2}}, \quad \lambda_3$$

corresponding to the following kinetic eigenvectors:

$$V_i^{(0)} = 1, \quad W_i^{(1)} = (c_{ix}\cos\theta - c_{iy}\sin\theta),$$

$$W_i^{(2)} = (c_{ix}\sin\theta + c_{iy}\cos\theta), \quad V_i^{(3)} = c_{ix}^2 - c_{iy}^2.$$

The eigenvectors $W^{(1)}$ and $W^{(2)}$ are obtained by rotating c_{ix} and c_{iy} by the angle θ defined by the local flow velocity, $u_x = u\cos\theta$, $u_y = u\sin\theta$. When the flow is at rest ($u = 0$), this transformation degenerates and one goes back to the standard eigenvectors $V_i^{(k)}$.

The numerical scheme is stable for all values of D^* and u^* such that the eigenvalues of Ω_{ij} lie in the interval $0 < \lambda_k < 2$, that is

$$0 < \frac{2(1-2u^{*2})}{1+4D^*-2u^{*2}} < 2, \quad 0 < \lambda_3 < 2.$$

This implies $u^{*2} < 1/2$, namely Mach number $Ma^2 = u^{*2}/c_s^2 < 1$, regardless of the value of $D^* > 0$. On the other hand, due to the near-equilibrium approximation, it is clear that for very small values of D^*, such that λ_2 and λ_3 come near to the upper bound 2, the scheme exhibits long-lasting oscillations which may hamper the numerical efficiency of the method. Contrary to the MLW method and single-time relaxation method, a 4-point template is sufficient to remove flow-dependent numerical diffusion. It is worth stressing that this is only possible thanks to the off-diagonal elements of the matrix Λ, which serve precisely the purpose of absorbing artificial directional effects due to the combined effect of lattice discreteness and multidimensional flow ($u_x u_y \neq 0$).

3. Numerical simulations

In the following, we present some test simulations to validate the kinetic scheme and compare it with a finite-difference Modified Lax-Wendroff scheme.

3.1. Isotropic diffusion: (D = constant, $\vec{u} = 0$)

We consider the time evolution of a Gaussian density profile under the effect of a constant diffusion and no flow, that is zero cell-Peclet number $Pe_c = U\delta_x/D$.

The initial distribution is given by

$$\rho(\vec{r},0) = \frac{\rho_0}{2\pi\sigma_0^2}\exp\left(-\frac{|\vec{r}-\vec{r}_0|^2}{2\sigma_0^2}\right). \tag{12}$$

The results of the simulation for the case $\sigma_0 = 10$, $\rho_0 = 10^3$ on a 250×250 grid, are summarized in Table 1. Table 1 reports the L_2 and L_∞ deviations from the exact solution of both LB and MLW schemes at time $t = 100$ (physical units). These deviations are defined as:

$$\|\delta\rho\|_2 = \left(\frac{1}{N}\sum_{x,y}|\rho(x,y)-\rho^{\text{exact}}(x,y)|^2\right)^{1/2}$$

and

$$\|\delta\rho\|_\infty = \max_{(x,y)}\{|\rho(x,y)-\rho^{\text{exact}}(x,y)|\},$$

where N is the number of grid points.

In order to stress the stability limit of the kinetic scheme, the lattice diffusivity can be chosen ten times higher than the one of the modified Lax-Wendroff scheme, that is $D^*_{\text{LB}} = 2.5$ and is $D^*_{\text{MLW}} = 0.25$ (first row of Table 1), so that a corresponding ten-fold larger time-step can be used in the kinetic scheme, at a given value of the physical diffusion coefficient ($D = 1$). To be noted that $D^* = 2.5$ is beyond the critical value for the MLW method, as indicated by the empty entries in the MLW columns. The numerical results show satisfactory agreement with the analytical solution, with a fast decay of the error with the time-step followed by a saturation when the amplitude falls below $\approx 10^{-5}$. Timing data indicate that the kinetic LB scheme can compute significantly faster than MLW.

It is also instructive to assess the non-isotropy error associated with the single-time relaxation scheme (lattice BGK or LBGK for short), as opposed to present matrix formulation. These are shown in Table 2. This table shows that, according to the expression (9), the isotropy error of the 4-speed LBGK scheme

Table 1
Comparison of the LB and MLW methods for the case of pure diffusion ($D = 1$, $\lambda_3 = 1$)

δ_t	LB L_2	MLW L_2	LB L_∞	MLW L_∞
2.5	2.78×10^{-2}	-1.56×10^{-2}	–	
1	3.26×10^{-3}	-1.83×10^{-3}	–	
0.5	7.02×10^{-4}	–	4.12×10^{-4}	–
0.25	2.27×10^{-5}	2.27×10^{-5}	2.94×10^{-4}	2.94×10^{-4}
0.1	3.10×10^{-5}	6.8×10^{-6}	3.47×10^{-4}	5.76×10^{-5}
0.01	3.84×10^{-5}	2.18×10^{-5}	4.28×10^{-4}	2.80×10^{-4}

Table 2
Isotropy error for the MLW, LB and LBGK method, $\lambda_3 = 1$

$\vec{u}$	D^*_{theor}	Pe	D^*-measured value			
			MLW	LB	LBGK-4	LBGK-9
(0.2, 0.2)	0.20	1.41	0.200	0.200	0.186	0.200
(0.2, 0.2)	2.00	0.141	–	2.00	1.82	2.000
(0.1, 0.1)	0.20	1.41	0.200	0.200	0.198	0.200
(0.2, 0.2)	2.00	0.141	–	2.00	1.97	2.000

is of order Ma^2. It is worth noting that by adding four populations moving along the next-to-nearest neighbor (diagonal) connections, plus one population of rest particles, the LBGK scheme (see column LBGK-9, which stands for LBGK with nine populations) does in fact recover isotropy. However, this recovery comes at the expense of a factor 9/4 in the number of variables. In addition, since the diffusivity is fixed by the a single relaxation parameter, ω, it is clear that the 9-speed LBGK scheme cannot deal with genuinely anisotropic problems.

3.2. Non-isotropic diffusion ($D_{xx} \neq D_{yy} \neq D_{xy}$, $\vec{u} = 0$)

A distinctive feature of the present matrix LB scheme is the capability to simulate non-isotropic diffusion phenomena. Such phenomena play a major role in a variety of applications, involving ferrofluids, liquid crystals and biological flows [15]. The non-isotropic capabilities of the present method are demonstrated in Table 3, for two typical anisotropy ratios $D_{\max}/D_{\min} = 2$ and $D_{\max}/D_{\min} = 10$, which can be taken as representative of nematic and smectic regimes, respectively [15,16]. The initial distribution was taken in the same form as in the previous section, (12). The analytical solution is then

$$\rho(\vec{r}, t) = \frac{\rho_0}{2\pi\sqrt{\|\sigma_{\alpha\beta}\|}} e^{2(\sigma^{-1})_{\alpha\beta} r_\alpha r_\beta}, \quad \sigma_{\alpha\beta} \equiv \sigma_0^2 \delta_{\alpha\beta} + 2tD_{\alpha\beta}. \tag{13}$$

From this table, we see that the present method can handle fairly significant anisotropy ratios. In addition, as shown in the last two rows, it can also handle arbitrary rotations of the lattice ($\pi/6$ for the case in point). This non-isotropic capability, combined with the fact that the diffusion tensor is allowed to change

Table 3
Error of the LB method for the case of non-isotropic diffusion ($\delta_t = 0.25$, $\lambda_3 = 1$, $t = 100$, $\sigma_0 = 10$, grid 250×250)

D_{xx}, D_{yy}, D_{xy}	LB L_2	LB L_∞
$1, \frac{1}{2}, 0$	4.00×10^{-5}	5.40×10^{-4}
$1, \frac{1}{10}, 0$	4.12×10^{-5}	5.45×10^{-4}
$\frac{7}{8}, \frac{5}{8}, -\frac{\sqrt{3}}{8}$	3.97×10^{-5}	5.35×10^{-4}
$\frac{31}{40}, \frac{13}{40}, \frac{9\sqrt{3}}{40}$	4.20×10^{-5}	6.13×10^{-4}

Table 4
Taylor–Aris dispersion, the width of the channel is 48

Pe_c	D^*	U_c^*	$D_L/D - 1$	$Pe^2/470$	Error (%)
0.1	0.25	0.025	0.0486	0.0490	0.8
0.5	0.125	0.0625	1.221	1.226	0.3
1.0	0.25	0.25	4.89	4.90	0.2
5	0.05	0.25	121.5	22.6	0.9
10	0.05	0.5	487.5	490.2	0.6

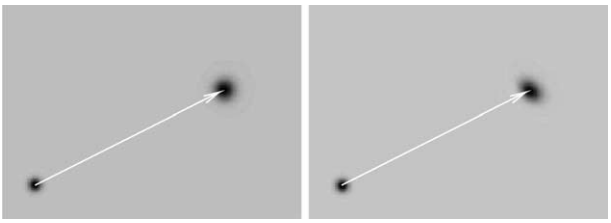

Fig. 1. Plots of the density distribution at $t = 0$ and $t = 1100$ (arrow tail and head, respectively) for the present LB (left) and MLW (right).

in space and time, makes the present kinetic scheme a good candidate for the numerical simulation of diffusion and heat transport phenomena in anisotropic media, with and without accompanying fluid flow and external fields [17].

3.3. Diffusion–advection

Next we test the kinetic LB scheme for the case of diffusion and advection in a prescribed flow configuration.

We have simulated the standard Taylor–Aris dispersion problem at various global Peclet numbers, $Pe = U_c L/D$, U_c being the centerline speed of the parabolic flow profile, and checked against the analytical expression for the longitudinal dispersion coefficient

$$D_L = D\left(1 + \frac{Pe^2}{470}\right).$$

The initial conditions are Gaussian, with width $\sigma_x = 5$ and $\sigma_y = 50$. The time-span of the simulations ranged from 2000 to 10,000 time-steps depending on the Peclet number. The results, for channels of width 48 lattice units and lengths ranging from 500 to 2000, are reported in Table 4.

Again, satisfactory agreement with analytical results is observed up to $Pe_c \sim 10$, which is fairly adequate for many practical applications. In order to test isotropy issues, we consider the case of a genuinely 2D flow, $u_x^* = 0.2$ and $u_y^* = 0.1$, in a free (periodic) domain of size 350×250. The other parameters of the simulation are, $\sigma_0 = 5$, $D_{LB}^* = D_{MLW}^* = 0.02$, corresponding to a cell-Peclet $Pe_c = 11.2$.

In Fig. 1 plots of the density are shown at time $t = 0$ and $t = 1100$ for both LB and MLW methods. As expected, numerical data (see white arrows) follow the exact expression $\langle \vec{r}(t) \rangle = \vec{r}_0 + \vec{u}t$, where brackets stand for integration over the density distribution over the flow domain.

From Fig. 1 it is apparent that, while the MLW results show visible deviations from isotropy, the present matrix LB method proves nearly free of spurious directional effects.

Quantitative analysis of contour lines in the form $r = r(\theta)$ at $\rho = (1/e)\rho_{max}$, delivers a non-isotropy factor $\rho_{max}/\rho_{min} = 1.74$ for MLW and $\rho_{max}/\rho_{min} = 1.02$ for LB (clearly, for the isotropic case $\rho_{max}/\rho_{min} = 1$).

4. Conclusions

A matrix kinetic scheme for advection–diffusion problems has been proposed. Besides being able to deal with genuinely anisotropic problems, such matrix formulation permits to tame artificial directional effects due to lattice discreteness in the presence of two dimensional flow. The method is also compared with a modified Lax-Wendroff scheme, and found capable of marching in much larger time-steps, due to the absence of diffusive Courant stability constraints. On the other hand, the kinetic LB method is restricted to low-gradient conditions, i.e., the fluid flow and density profiles should not vary appreciably on the scale of a single lattice spacing. In addition, the LB method requires four moving species for a single physical species, with a corresponding increase of memory occupation. For fully coupled fluid-advection–diffusion problems, in which the fluid flow needs also to be computed, such memory limitation is much less severe than it appears. A two dimensional LB–MLW calculations requires 9 + 1 = 10 arrays, against the 9 + 4 = 13 arrays required by a LB–LB approach, which means just a 30% increase. Similar figures apply in 3D, with 15 + 1 = 16 versus 15 + 6 = 21 for the LB–MLW and LB–LB, respectively. In addition, a further factor 2 savings comes from the fact that kinetic schemes only require one time level of storage, since the state of the system at the previous time step can be overwritten 'on the fly', i.e., while advancing the solution in time at each lattice site. It is therefore expected that the minor memory overhead of the LB–LB approach is more than compensated by the significant gains in the size of the time-step. On the other hand, as compared to existing single-time relaxation schemes, the present matrix formulation permits to address genuinely non isotropic problems. It can also cure spurious directional effects which affect nearest-neighbor LBGK schemes even for physically isotropic problems.

Summarizing, we have presented a matrix kinetic scheme for diffusion–advection problem with the following features:

(i) It can march in larger time steps than scalar (non-kinetic) explicit methods, such as modified LW and Moment Propagation methods, because the time step is free of diffusive CFL constraints.
(ii) It can handle non-isotropic problems, which are by definition out of reach for single-time relaxation kinetic schemes. Moreover, it can also cure spurious anisotropic effects which affect nearest-neighbor single-time relaxation kinetic methods even for the case of isotropic problems.
(iii) It achieves (i) and (ii) without introducing any memory overhead as compared with existing kinetic schemes.

Acknowledgements

S.S. is grateful to the Alexander von Humboldt Foundation for financial support. He acknowledge kind hospitality at the Institute for Crystal Growth, Berlin, where this work was performed.

Appendix A. Isotropy of LBGK scheme with nine speeds

Let us consider a LBGK scheme with the following nine discrete speeds:

$$\vec{c}_0 = (0,0),$$
$$\vec{c}_1 = (1,0), \quad \vec{c}_2 = (0,1), \quad \vec{c}_3 = (-1,0), \quad \vec{c}_4 = (0,-1),$$
$$c_5 = (1,1), \quad c_6 = (1,-1), \quad c_7 = (-1,-1), \quad c_8 = (-1,1).$$

The equilibrium distribution is defined as follows:

$$f_i^{\mathrm{eq}} = w_i\rho\left(1 + \frac{u_\alpha^* c_{i\alpha}}{c_s^2} + \frac{Q_{i\alpha\beta}u_\alpha^* u_\beta^*}{2c_s^4}\right),$$

where $Q_{i\alpha\beta} \equiv c_{i\alpha}c_{i\beta} - c_s\delta_{\alpha\beta}$ and $c_s^2 = \sum_i w_i c_{ix}^2 = \sum_i w_i c_{iy}^2$ is the lattice sound speed, w_i being a set of weights normalized to 1.

Taylor expansion of the Eq. (2) yields the system of two hyperbolic equations for ρ and $\vec{\mathbf{J}}$:

$$\dot{\rho} + \nabla_\alpha \mathbf{J}_\alpha + \tfrac{1}{2}\ddot{\rho}_i + \nabla_\alpha \dot{\mathbf{J}}_\alpha + \tfrac{1}{2}\nabla_\alpha\nabla_\beta \mathbf{P}_{\alpha\beta} = \omega(\rho^{\mathrm{eq}} - \rho), \tag{A.1}$$

$$\dot{\mathbf{J}}_\alpha + \nabla_\beta \mathbf{P}_{\alpha\beta} + \tfrac{1}{2}\ddot{\mathbf{J}}_\alpha + \nabla_\beta \dot{\mathbf{P}}_{\alpha\beta} + \tfrac{1}{2}\nabla_\beta\nabla_\gamma \mathbf{M}_{\alpha\beta\gamma} = \omega(\mathbf{J}_\alpha^{\mathrm{eq}} - \mathbf{J}_\alpha), \tag{A.2}$$

where all symbols have the same meaning as in the main text. Next, we assume that $\mathbf{P}$ and $\mathbf{M}$ are near their equilibrium values:

$$\mathbf{P}_{\alpha\beta} \approx \mathbf{P}_{\alpha\beta}^{\mathrm{eq}} = \rho\sum_i w_i c_{i\alpha}c_{i\beta}\left(1 + \frac{Q_{i\gamma\delta}u_\gamma^* u_\delta^*}{2c_s^4}\right) = \rho\left(c_s^2\delta_{\alpha\beta} + \frac{u^{*2}}{2c_s^2}\left(\frac{1}{3} - c_s^2\right) + \frac{1}{3}\frac{u_\alpha^* u_\beta^*}{c_s^2}\right),$$

$$\mathbf{M}_{\alpha\beta\gamma} \approx \mathbf{M}_{\alpha\beta\gamma}^{\mathrm{eq}} = \rho c_s^2 u_\delta^*\delta_{\alpha\beta\gamma\delta}.$$

The previous expressions were obtained with the only assumption that $w_+ = 4w_\times$, where subscripts + and × denote nearest-neighbor and next-to-nearest neighbor connections, respectively. We note that for $c_s^2 = 1/3$ one recovers the usual isotropic expression of the equilibrium pressure tensor, $\mathbf{P}_{\alpha\beta}^{\mathrm{eq}} = \rho(c_s^2\delta_{\alpha\beta} + u_\alpha^* u_\beta^*)$. The value $c_s^2 = 1/3$ can be achieved by choosing $w_0 = 4w_+$, which yields the standard set of weights for 9 speed LBGK schemes [18]:

$$w_0 = \tfrac{4}{9}, \quad w_+ = \tfrac{1}{9}, \quad w_\times = \tfrac{1}{36}.$$

By assuming that $\dot{\mathbf{J}}_\alpha^{\mathrm{eq}} \approx -u_\alpha^* u_\beta^*\nabla_\beta\rho$ and $\ddot{\rho} \approx u_\alpha^* u_\beta^*\nabla_\alpha\nabla_\beta\rho$, Eqs. (A.1) and (A.2) transform into:

$$\dot{\rho} + \nabla_\alpha u_\alpha^*\rho + \nabla_\alpha \mathbf{J}_\alpha^{\mathrm{neq}} - \tfrac{1}{2}u_\alpha^* u_\beta^*\nabla_\alpha\nabla_\beta\rho + \tfrac{1}{2}(c_s^2\delta_{\alpha\beta} + u_\alpha^* u_\beta^*)\nabla_\alpha\nabla_\beta\rho = 0,$$
$$-u_\alpha^* u_\beta^*\nabla_\beta\rho + \nabla_\beta\rho(c_s^2\delta_{\alpha\beta} + u_\alpha^* u_\beta^*) = -\omega\mathbf{J}_\alpha^{\mathrm{neq}}.$$

It is thus seen that the additional diffusion disappears from these equations, and we are left with:

$$\dot{\rho} + \nabla_\alpha u_\alpha^*\rho + \nabla_\alpha \mathbf{J}_\alpha^{\mathrm{neq}} + \tfrac{1}{2}c_s^2\Delta\rho = 0, \tag{A.3}$$

$$c_s^2\nabla_\alpha\rho = -\omega\mathbf{J}_\alpha^{\mathrm{neq}}, \tag{A.4}$$

which deliver the desired advection–diffusion equation, with diffusivity

$$D^* = c_s^2\left(\frac{1}{\omega} - \frac{1}{2}\right).$$

References

[1] R. Benzi, S. Succi, M. Vergassola, The lattice Boltzmann equation: theory and applications, Phys. Rep. 222 (1992) 145–197.
[2] S. Succi, The Lattice Boltzmann Equation for Fluid Dynamics and Beyond, Clarendon Press, Oxford, 2001.
[3] D. Wolf-Gladrow, Lattice-Gas Cellular Automata and Lattice Boltzmann Models, Springer, Berlin, 2000.
[4] S. Chen, G.D. Doolen, Lattice Boltzmann method for fluid flows, Annu. Rev. Fluid Mech. 30 (1998) 329–364.
[5] S. Succi, I. Karlin, H. Chen, Role of the H-theorem in lattice Boltzmann hydrodynamic simulations, Rev. Mod. Phys. 74 (2002) 1203.

[6] S. Succi, H. Chen, C. Teixeira, G. Bella, A. Mario, K. Molvig, An integer lattice realization of a Lax scheme for transport processes in multiple component fluid flows, J. Comput. Phys. 152 (1999) 493–516.
[7] A. Calì, S. Succi, A. Cancelliere, R. Benzi, M. Gramignani, Diffusion and hydrodynamic dispersion with the lattice Boltzmann method, Phys. Rev. A 45 (1992) 5771–5774.
[8] R.G.M. van der Sman, M.H. Ernst, Diffusion lattice Boltzmann scheme on an orthorhombic lattice, J. Stat. Phys. 94 (1999) 766–782.
[9] R.M.H. Merks, A.G. Hoekstra, P.M.A. Sloot, The moment propagation method for advection–diffusion in the lattice Boltzmann method: validation and Péclet number limits, J. Comput. Phys. 183 (2002) 563–576.
[10] X. Shan, G. Doolen, Diffusion in a multicomponent lattice Boltzmann equation model, Phys. Rev. E 54 (1996) 3614–3620.
[11] R.S. Maier, D.M. Kroll, H.T. Davis, R.S. Bernard, Pore-scale flow and dispersion, Int. J. Mod. Phys. C 9 (1998) 1523.
[12] W.F. Ames, Numerical Methods for Partial Differential Equations, third ed., Academic Press, New York, 1992.
[13] F. Higuera, S. Succi, R. Benzi, Lattice gas-dynamics with enhanced collisions, Europhys. Lett. 9 (1989) 345–349.
[14] M. Bouzidi, D. d'Humières, P. Lallemand, L.-S. Luo, Lattice Boltzmann equation on a two-dimensional rectangular grid, J. Comput. Phys. 172 (2001) 704–717.
[15] J. Ruohonen, M. Ylihautala, J. Jokisaari, ^{129}Xe diffusion in a ferroelectric liquid crystal, Mol. Phys. 99 (9) (2001) 711–719.
[16] C. Denniston, D. Marenduzzo, E. Orlandini et al., Lattice Boltzmann algorithm for three-dimensional liquid-crystal hydrodynamics, Phil. Trans. Roy. Soc. A 362 (2004) 1745–1754.
[17] G. Spiga, P. Vestrucci, S. Succi, Effects of anisotropic scattering on the distribution of charged particles in an electric-field, Il Nuovo Cimento 85 (1985) 208.
[18] Y. Qian, D. D'Humieres, P. Lallemand, Europhys. Lett. 17 (1992) 479.